Novel Techniques and Approaches to Unravel the Nature of X-Ray Absorption Spectra

F.M.F. de Groot

Department of Chemistry, Utrecht University, Sorbonnelaan 16, 3584 CA Utrecht, Netherlands

Abstract. This paper discusses the role of resonant inelastic X-ray scattering (RIXS) to unravel the nature of the states that are visible in the pre-edge region of the 3d metal K edges. The traditional pre-edge analysis into quadrupole transitions to the 3d-states plus dipole transitions to the 4p states is outlined, with special attention to the situation of TiO_2. The general possibilities of RIXS are described, including the various possible cross-sections through the 2D RIXS plane. Recent developments in High-Energy Resolution Fluorescence Detection (HERFD) are discussed, that yield XANES-like spectra with unprecedented resolution. Using the 1s2p RIXS of $LiCoO_2$ as example, the presence of an extra peak due to non-local dipole transitions is explained. The non-local nature of this dipole pre-edge peak is proven from its behavior in the 2D RIXS plane. The paper also discusses a range of selective X-ray absorption experiments, where the selectivity is towards (a) the spin-state, (b) the valence, (c) the neighbor atom and (d) the edge. In the outlook, a number of additional experimental routes is suggested, which shows that the use of RIXS, HERFD and selective XAS techniques is only just starting.

Keywords: X-ray absorption, π-bonding, charge transfer multiplet theory
PACS: 78.70.Dm

INTRODUCTION

The understanding of the shapes of the metal K edge X-ray absorption spectra of transition metal systems is based on the single-particle excitation model. In the X-ray absorption process an electron is excited from a core state to an empty state and the X-ray absorption cross section is essentially identified with the empty density of states, modified by the transition matrix element. The most popular codes to calculate the density of states of both molecules and solids are based on Density Functional Theory (DFT), for example FEFF [1], Wien2K [2] and many more. The 3d metal K edges can be separated into a pre-edge region and an edge region. The edge region identifies with the onset of the 4p conduction band and higher bands, whereas the pre-edge identifies with the 3d-band. Because the 3d-density is large, the quadrupole transitions are of the same order of magnitude as the dipole transitions and are visible in the spectrum. Figure 1 shows a ground state p-projected DOS of TiO_2, which corresponds closely with the overall K edge X-ray absorption spectrum. The pre-edge region shows the T_{2g} and E_g peaks in the calculation, which is in contrast to the K edge experiment that shows three peaks.

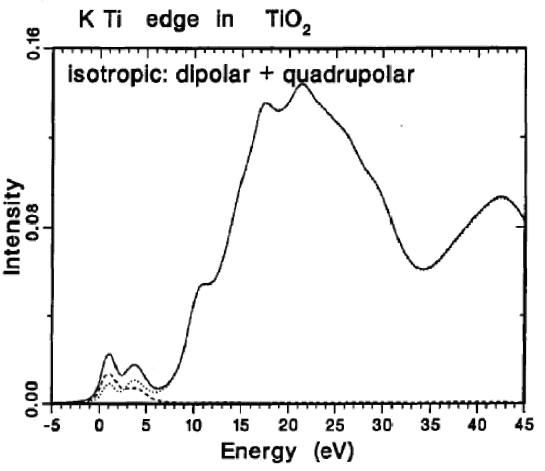

FIGURE 1. The titanium ground state p-projected DOS of TiO_2, indicating the pre-edge region between 0 and 5 eV and the edge starting at 10 eV. The pre-edge is separated into dipole (thin line) and quadrupole (dashed) transitions [3].

This discrepancy has been solved by a number of theoretical approaches. The main point is the presence of the core hole in the final state. The core hole effectively pulls down the quadrupole transitions to the 3d states by ~2.5 eV with respect to the 4p states that are hybridized into this 3d-band. This creates a pre-

CP882, *X-ray Absorption Fine Structure—XAFS13*
edited by B. Hedman and P. Pianetta

edge structure of 4 peaks. These states are split by a crystal field of 2.5 eV and a core hole potential of 2.5 eV, which makes the middle peak a combination of the E_g quadrupole and T_{2g} dipole peak. This general model has been used in a number of, theoretically slightly different, approaches by Shirley [4], Cabaret et al. [5] and Kotani [6], all with the same result and in close agreement with experiment.

The situation regarding iron K edge pre-edge structures seems rather different at first sight. The elegant analysis of Westre et al. shows the crystal field multiplet structures that form the basis for the iron pre-edge structures, in very good agreement with experiment. These experiments show only quadrupole peaks for octahedral systems and quadrupole plus dipole peaks for tetrahedral system, where in contrast to TiO_2 the quadrupole and dipole peaks are exactly the same energy. This is due to the fact that in tetrahedral symmetry the quadrupole and dipole transitions reach the same final state.

This leads to a number of questions we would like to solve in this paper, where we will make use of high-resolution fluorescence detection to increase the amount of information on pre-edge structures. The questions we would like to solve in this respect are:

1. Why is this shift visible for Ti-oxides and not for Fe-oxides?
2. What is the exact origin of the shift between dipole and quadrupole peaks?
3. What is the difference between octahedral versus tetrahedral systems?

RESONANT INELASTIC X-RAY SCATTERING

Before we return to the question mentioned above, resonant inelastic X-ray scattering (RIXS) is introduced. Using RIXS one can measure the K pre-edge structures in combination with, for example, the 1s2p decay. This yields much additional information with regard to the nature of the pre-edge states [7]

The extra component of a RIXS experiment, with respect to an X-ray absorption experiment is a high-resolution fluorescence detector. This approach has been initiated by Hämäläinen et al., who used a high-resolution fluorescence detector to effectively remove the lifetime broadening [8]. This method allows in addition for the measurement of high-resolution X-ray emission spectra, either on- or off-resonance. Caliebe et al. [9] measured the Kα emission spectra of Fe_2O_3 on the K pre-edge. Figure 2 shows an energy scheme of this experiment. Assuming that one can approximate the ground state of Fe^{III} as $3d^5$, the iron K pre-edge consists of two quadrupole transitions, respectively adding a spin-down T_{2g} and an E_g electron to the five spin-up electrons, yielding two $1s13d^6$ states. The resonant Kα emission effectively replaces a 1s core hole with a 2p core hole, which in turn leads to a $2p53d^6$ configuration. This $2p53d^6$ final state is identical to the final state in 2p X-ray absorption. Charge transfer multiplet calculations indeed confirm his qualitative picture [10].

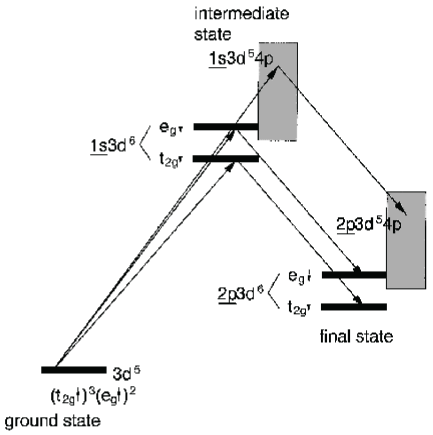

FIGURE 2. The transitions in the pre-edge region of the iron K edge, followed by the K_α fluorescence decay in Fe_2O_3.

If one combines the spectra of the X-ray absorption and X-ray emission experiments, one obtains a two-dimensional image that describes the full RIXS experiment in a certain energy range.

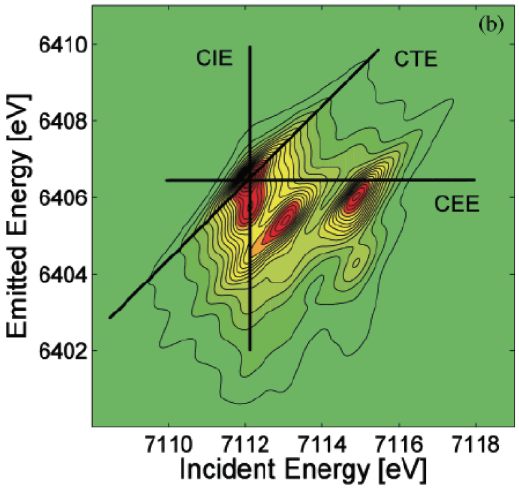

FIGURE 3. The 2D RIXS image of a CTM calculation of the tetrahedral Fe^{II} compound Fe_2SiO_4. The horizontal axis shows the excitation energy and the vertical axis the energy of the emitted X-ray [11].

Figure 3 shows the 2D image of the tetrahedral divalent iron system Fe_2SiO_4. The $3d^6$ ground state is excited to a $1s^1 3d^7$ intermediate state and decays to a $2p^5 3d^7$ final state [11]. This 2D image provides extra information with respect to the pre-edge spectrum alone. The pre-edge spectrum can be obtained from this 2D image as the integral of the complete structure. The Kα X-ray emission from the edge and energies above the edge occurs at a constant emitted energy, given by the energy difference between a 1s and a 2p core state. At the pre-edge, variations in the emitted energy occur as can be seen in Figure 3. Some pre-edge states emit at slightly different energies. In this respect it is interesting to look at the different cross sections through Figure 3. The Constant Transferred Energy (CTE) line corresponds, at resonance!, to states that decay to the same final state, which is given by the energy difference of excitation minus decay energy. From Figure 3 it is clear that the different states in the excitation do not decay to the CTE line. This indicates that due to symmetry and matrix element effects, they decay to different final states. If two states decay to the same emitted energy, i.e. on the same CEE line, this implies that the energy difference in the excitation is maintained in the decay. This behavior is default above the edge because the excited photoelectron effectively takes away the energy difference, but at the pre-edge resonance it implies that, for example, the energy difference between a T_{2g} and an E_g state is maintained in the decay step. The detailed comparison between crystal field theory and experiment of the complete 2D RIXS images of a number of iron oxides yielded very good agreement, with the exception of Fe_2O_3 [11].

HIGH-ENERGY RESOLUTION FLUORESCENCE DETECTION XANES

The CEE line in Figure 3 is in fact the experimental cross section that has been used by Hamalainen et al. to remove the lifetime broadening. Figure 3 shows that, at resonance, the CEE curve is not exactly identical to the X-ray absorption, as the emission resonances are slightly displaced. However, in all cases studied so far these energy shifts are below 1 eV. This also implies that if one measures with an experimental resolution of 1 eV these effects disappear and one measures a spectrum equivalent to the XANES spectrum.

Figure 4 shows the HERFD-XANES spectrum of Fe_2SiO_4 compared with the normal XANES spectrum. One observes a clear improvement of the pre-edge structure. This improvement is important for the qualitative usage of the pre-edge structure for the determination of the valence and site symmetry. Wilke et al have shown that, in case of iron, the average energy (i.e. its center-of-gravity) is linear with valency and the intensity determines the site symmetry, octahedral versus tetrahedral. From figure 4 it is obvious that the analysis of the HERFD-XANES spectra is far more accurate than the analysis of normal XANES. The analysis of a number of iron oxide references showed that the HERFD-XANES and normal XANES energies are identical, but that the normalized intensity of HERFD-XANES is systematically three times higher than that of normal XANES [12]. It is noted that HERFD-XANES is an experiment where a hard X-ray goes into the system and is emitted from the system. This makes it possible to perform experiments under extreme conditions, for example studying a catalyst during its synthesis and also under actual working conditions. This has been applied to FeZSM5 systems, where the gradual change from octahedral to tetrahedral Fe^{III} has been exposed [12].

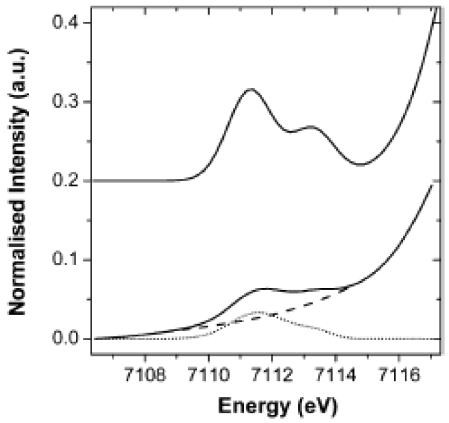

FIGURE 4. The comparison of a normal XANES (bottom) and HERFD-XANES spectrum (top) of the iron K pre-edge region of Fe_2SiO_4.

In contrast to the identical results for iron, the HERFD-XANES and XANES analysis yields completely different results in case of manganese. Farges et al. [13] determine an energy shift of 0.3 eV between MnO and Mn_2O_3 using normal XANES, whereas Glatzel et al. find an energy shift of 2.0 eV[14]. The reason for this large discrepancy lies in the complex $1s^1 3d^5$ multiplet structure for the Mn^{III} final state.

Figure 5 shows the multiplets structures of the pre-edges of 3d-systems as calculated from a single $3d^N$ configuration. It can be seen in Figure 5 that a (Fe^{II}) $3d^5$ and (Fe^{II}) $3d^6$ ground state give well defined structures in a relatively short energy range of 4 eV. In

contrast, a $3d^4$ ground state (Mn^{III}) yields a multiplet structure that is spread over 7 eV and in addition has small lobes at its extremes. These features make the $3d^4$ ground state very difficult to analyze. It turns out that in normal XANES only the center part of the multiplet structure is visible, while in HERFD-XANES the wider multiplet becomes visible. This difference is the reason for the discrepancy between XANES and HERFD-XANES analysis for $3d^4$ Mn^{III} systems.

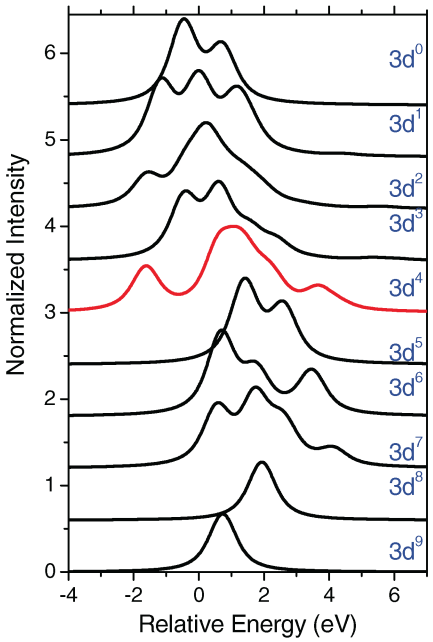

FIGURE 5. The multiplet structures of the pre-edges of 3d-systems. The top spectrum is given by the calculation from $3d^0$ to $1s^13d^1$. The other $3d^N$ ground states are indicated on the right.

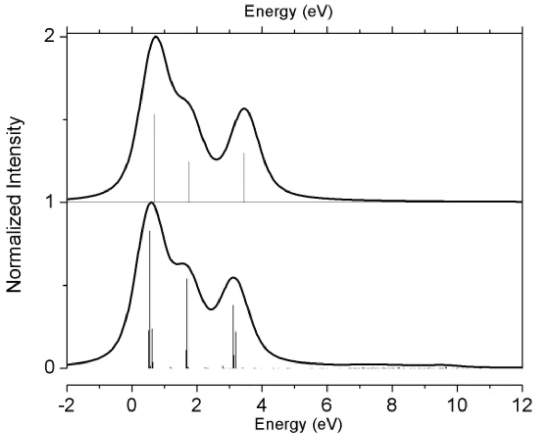

FIGURE 6. (top) Crystal field multiplet calculation for the transition from $3d^5$ to $1s13d^6$. (bottom) Charge transfer multiplet calculation, using the CTM parameters of Fe_2SiO_4.

The use of a single configuration as used in Figure 5 and by Westre et al [15] is justified because charge transfer effects are very small for the spectral shapes of K pre-edges. Figure 6 shows the comparison of a single $3d^6$ configuration (crystal field multiplet) calculation and a two configuration $3d^6 + 3d^7\underline{L}$ (charge transfer multiplet) calculation.

NON-LOCAL EFFECTS IN THE PRE-EDGES OF 3D TRANSITION METALS

We now return to the questions as mentioned in the introduction. The Fe and Mn pre-edge structures are complex and need multiplet calculations for a detailed simulation, but their complete pre-edge structure can be calculated by the quadrupole transition from $3d^N$ to $1s^13d^{N+1}$. There seems to be no sign of the shifted dipole, as observed for TiO_2. The dipole peak in TiO_2 can be understood as being caused by a non-local (screening) effect. The 1s electron is excited to an empty p-symmetry state that is part of the 3d-band. This can be understood as follows: The Ti 3d band is very strongly hybridized with its oxygen neighbors. This implies a large amount of ligand holes on the oxygen sites. These ligand holes also interact very strongly with 4p states of another titanium atom. The transition can then be envisioned as a transition to a 4p state that is part of the 3d-band due to its overlap, via oxygen, with another titanium. The transition can be written as $3d^0$ to $1s^14p^1(3d)$. Because the electron is part of a delocalized band, the core hole effect is much smaller than for a local $1s^13d^1$ configuration, which is the reason for the shift between dipole and quadrupole. This interpretation is confirmed by the L edges of isolated Ti ions that only show quadrupole transitions and no non-local dipole transitions [16].

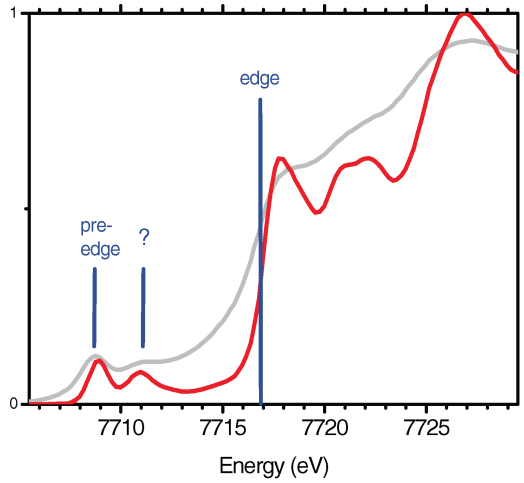

FIGURE 7. The K edge of $LiCoO_2$ measured with HERFD-XANES (red) and normal XANES (light grey).

There is no reason to assume that these non-local effects should not be a general phenomenon, so why are they not seen in other pre-edge spectra and 2D RIXS images? They have been recognized recently for Cu RIXS spectra [17]. New cobalt 1s2p RIXS data measured with 0.3 eV resolution by Vanko et al. [18] shows very clear evidence of this non-local peak.

Figure 7 shows the K edge XANES spectrum of $LiCoO_2$. The edge is visible 7717 eV and before the edge two separate peaks are visible at respectively 7709 eV and 7711 eV, where the HERFD-XANES shows two well separated peaks. The clearest evidence for the non-local dipole peak is in the 1s2p RIXS images of $LiCoO_2$ in combination with another low-spin Co^{III} oxide $EuCoO_3$. Because low-spin $3d^6$ has a filled T_{2g} shell and an empty E_g shell, their quadrupole spectra consist of only a single peak. In the HERFD-XANES spectra two peaks are visible. The 1s2p RIXS images show that the first peak has a broadening symmetric with the CIE axis and the second structure is symmetric with the CEE axis. This implies that the first peak is a $3d^6 \rightarrow 1s^1 3d^7 \rightarrow 2p^5 3d^7$ local resonance, while the second peak is a $3d^6 \rightarrow 1s^1 4p^1$(3d-band)$\rightarrow 2p^5 4p^1$(3d-band) transition that occurs at a fixed emission energy. Even clearer evidence is given by the relative ratios of both peaks: $LiCoO_2$ is dominated by the quadrupole peak, whereas $EuCoO_3$ is dominated by the non-local dipole peak. There is a direct relation between the relative importance of the non-local dipole peak and the possibilities for coupling of the empty 4p-states into neighboring 3d-bands, where the Co-O-Co is crucial, as is explained in detail by Vanko et al.[18].

The new general model to describe the pre-edges of 3d transition metals reads as follows:

1. The pre-edge is caused by quadrupole transitions from 1s to 3d, while the edge is caused by dipole transitions from 1s to 4p.
2. There is a non-local dipole peak that is caused by transition to the 4p states that are hybridized into the 3d-band. The hybridization is via oxygen to the nearest metal neighbor, where its strength is determined by the geometry and degree of covalence. Because this final state is less localized it is not as much affected by the core hole potential as the localized 3d-states.
3. If point symmetry is broken, as for example in tetrahedral symmetry, there is local mixing of the 4p and 3d states, yielding local dipole transitions into the localized 3d-states. In this case there are localized, mixed, 3d4p states that, being a single state, must be at the same energy.

In addition to the TiO_2 case and the Cu RIXS, there are hints of this non-local peak in many pre-edge spectra. Low-spin Fe^{II} systems have the same T_{2g}^6 ground state and Westre et al. indeed recognize an additional peak between the pre-edge and the edge[15], which in this new model identifies with the non-local dipole peak. The non-local dipole peak also seems to be dominant in the Fe_2O_3 pre-edge and RIXS spectrum, which does not correspond well to pure quadrupole calculations.

SELECTIVE X-RAY ABSORPTION EXPERIMENTS

A very interesting application of the use of high-resolution fluorescence detectors is the measurement of selective X-ray absorption spectra. The concept is simple: put the detector at an X-ray emission line for a specific state and only this state is observed. Its X-ray absorption spectrum can be measured, which then yields a selective X-ray absorption spectrum. To date, selective X-ray absorption has used to separate spin-states, valence states and L_2 from L_3 edges. In principle other selection criteria could be invoked as will be introduced below. Also non-radiative (Auger) decay channels could be used for this purpose.

The first series of selective X-ray absorption experiments focused on the 1s3p (K_β) X-ray emission channel in order to separate spin-up from spin-down states. It can be shown that the excitation of a spin-up 1s electron is different from the excitation of a spin-down 1s electron. In the multiplet calculations this effect can be calculated if one uses the small 1s3d exchange interaction in the intermediate state to calculate the 1s3p decay. In case of a Mn^{II} $3d^5$ ground state, the 1s3d exchange interaction creates two states, respectively with ^5S and ^7S atomic symmetry. It can be shown that the difference in spectral shape between these two states is exactly the difference between spin-up and spin-down, which provides a tool to measure the spin-polarized XANES spectrum. Because XANES is a local probe this spin-polarized XANES is also local with respect to the 3d spins, implying that only the spin is detected and the same signal is found for para-, ferro-, and antiferro-magnetic systems [19,20].

Spin-polarized X-ray absorption measurements on ferromagnetic systems will provide the spin-polarized empty DOS. This property can also be measured with X-MCD if multiplied by the Fano factor. A measurement of both the spin-polarized XAS and the

X-MCD signal should provide the energy dependence of the Fano factor [21].

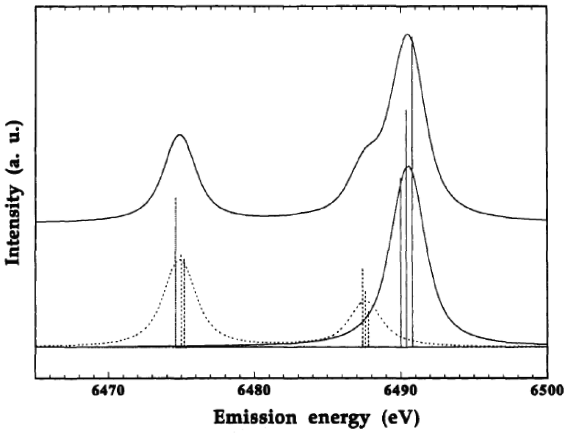

FIGURE 8. (top) Atomic multiplet calculations for $1s^1 3d^5$ to $3p^5 3d^5$ transition.. The solid line corresponds to a ^7S ground state and the dashed line to ^5S.

An important application of selective X-ray absorption is the use of the chemical shifts in the various X-ray emission channels. This yields the possibility to measure the valence selective X-ray absorption spectra, both the XANES and the EXAFS. This has been applied successfully to Fe^{III} as test-case [22]. The selective XAS tool has not been widely applied yet and many more options are available, at least in theory. For example, because a metal will have a different X-ray emission spectrum than an oxide, this difference can be used to measure the difference in X-ray absorption spectra for the metal respectively the oxide in a mixed system.

The distinction between a metal and an oxide can also been made using the so-called cross-over peaks [23]. In an oxide a peak is visible at ~20 eV binding energy and this energy indicates that it is related to the oxygen 2s state, which suggest that this X-ray fluorescence is a cross-over effect from an oxygen 2s state to metal 1s core state. The fact that this peak is visible is caused by hybridization of the oxygen 2s state with metal 4p states. This mixes some metal 4p character into the oxygen 2s state and this metal 4p-state decays to the 1s core hole. This interpretation is confirmed by the strong increase of intensity with shorter metal-oxygen distance [7].

Another interesting problem that can be tackled, in principle, with the selective XAS approach is the determination of the difference in neighbor atoms, for example to distinguish nitrogen from oxygen. Many coordination complexes, for example Cu^{II} Histidine complexes [24] have a coordination that is poorly known and/or varies with Ph and other properties of the solution and ligands. Selective XAS would be able to determine the relative abundance of oxygen versus nitrogen neighbors of the copper ion. This sensitivity is achieved by making use of the atomic multiplet calculations for $1s^1 3d^5$ to $3p^5 3d^5$ transition.. The solid line corresponds to a ^7S ground state and the dashed line to ^5S.

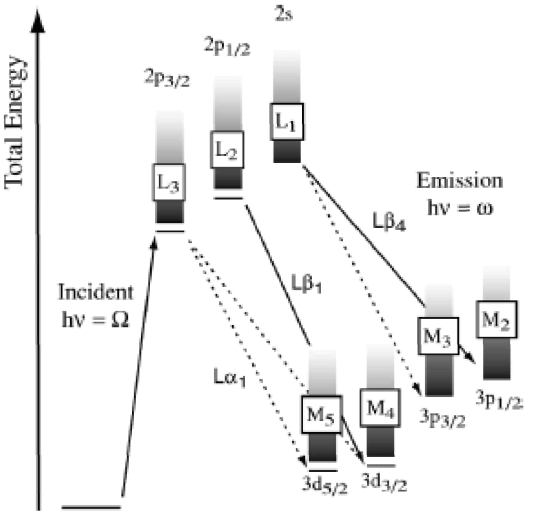

FIGURE 9. Energy scheme for *L* absorption and emission in rare earth systems. The discrete resonances before the edges indicate the strong 2*p*-5*d* transitions.

Selective X-ray absorption also allows one to measure an L_3 edge of a certain material, without seeing the L_2 edge, or the L_2 edge without the influence of the L_3 and the L_1 edge [25]. The mechanism behind this 'trick' is again the choice of one particular decay channel. If one measures a fluorescence channel that is specific for the L_2 edge, only the L_2 edge is observed. This is sketched in Figure 7. At first sight this looks like a perfect tool for the measurement of long K ranges because all other edges are invisible. This range extended EXAFS technique is however still affected by the other edges in the following way. If one excites the L_2 edge and measures its EXAFS through the L_1 edge, exactly at the L_1 edge there is a strong increase in the X-ray absorption cross section. This extra absorption is not detected, but it is still there, implying that the X-ray penetration depth becomes lower, which for a concentrated sample implies that the signal becomes smaller, i.e. one observes a dip instead of a peak at the L_1 edge. It can be shown that measurement on diluted (i.e. optically thin) samples solve this problem and thus provide a way to perform range extended EXAFS spectra. This technique is useful if the L edges are too close to each other to perform decent EXAFS, which is the case for the L edges from Ag to Gd.

CONCLUSIONS AND OUTLOOK

The development of high-resolution X-ray fluorescence detectors has yielded a range of new possibilities that are, slowly, being discovered.

The 2D RIXS images contain all the information for a certain excitation-decay combination, for example 1s2p (Kα) RIXS. Cross-sections and integrations through this image yield a series of interesting possibilities. Depending on the scientific questions at stake, one can optimize the measurements by selecting a certain cross-section. The experiments show that for optimal usage of the RIXS images, the overall resolution should be off the order of the lifetime broadening of the shallow core-hole, which is ~0.3 eV for 2p final states.

HERFD-XANES measures the XANES at fixed emission energy and as such provides a XANES-like spectrum with an energy resolution essentially determined by the experimental resolution. One can expect many applications to benefit from this approach. Important applications are the determination of the local electronic and magnetic structure of transition metal ions under in-situ or extreme conditions. This has been applied to catalysis and earth science, but in addition field such as mineralogy and bio-inorganic chemistry will benefit. In particular experiments under in-situ conditions for applications such as fuel cells, hydrogen storage and batteries are expected to benefit most in the future.

Selective X-ray absorption has been used to separate the spin, valence, neighbor atom and edge. This yields techniques such as spin-polarized XANES, valence selective XANES and range extended EXAFS. A large range of additional applications can be expected. As examples, I would like to mention the use of circular polarized X-rays in various combinations of X-MCD and HERFD-XANES. In principle one can use the L edge X-MCD contrast to measure the K edge X-MCD. This is essentially another route of measuring a soft x-ray spectrum with hard x-rays, with the obvious advantage of extreme conditions.

ACKNOWLEDGEMENTS

I would like to thank the many colleagues with whom I had to pleasure to work on RIXS experiments, in particular Pieter Glatzel, Uwe Bergmann, Gyorgy Vanko, Michael Krisch, Chi-chang Kao and Keijo Hämäläinen. Special thanks to Steve Cramer, who introduced me into the world of high-resolution X-ray detectors.

REFERENCES

1. J.J. Rehr and R.C. Albers, *Rev. Mod. Phys.* **72**, 621 (2000).
2. K. Schwarz, P Blaha and G.K.H. Madsen, *Comp. Phys. Comm.147*, **71** (2002)
3. F. M. F. de Groot, *J. Elec. Spec*. **67**, 529 (1994)
4. E. L. Shirley, *J. Elec. Spec*. 136, 77 (2004)
5. D. Cabaret, P. Sainctavit, P. Ildefonse, A.M. Flank, *J. Phys.* IV 7, 157 (1997)
6. T. Uozumi, A. Kotani, J.C. Parlebas, *J. Elec. Spec*. 137, 623 (2004)
7. P.Glatzel and U Bergmann, Coord. *Chem. Rev*. 249, 31 (2005).
8. K. Hämäläinen, D.P. Siddons, J.B. Hastings, L.E. Berman, *Phys. Rev. Lett*. 67, 2850 (1991)
9. W. A. Caliebe, C.-C. Kao, J. B. Hastings, M. Taguchi, A. Kotani, T. Uozumi, F.M.F. de Groot, *Phys. Rev. B.* **58**, 13452 (1998)
10. F. M. F. de Groot, *Chem. Rev.* 101 (2001) 1779 (2001)
11. F. M. F. de Groot, P. Glatzel, U. Bergmann, P.A. van Aken, R.A. Barrea, S. Klemme, M. Hävecker, A. Knop-Gericke, W.M. Heijboer, B.M. Weckhuysen, J. *Phys. Chem. B.* 109, 20751 (2005)
12. W. M. Heijboer, P. Glatzel, K.R. Sawant, R.F. Lobo, U. Bergmann, R.A. Barrea, D.C. Koningsberger, B.M. Weckhuysen and F. M. F. de Groot, *J. Phys. Chem. B.* 108, 10002 (2004)
13. F. Farges et al, *Phys. Rev. B*. 71, 155109 (2005)
14. P. Glatzel, U. Bergmann, J. Yano, H. Visser, J.H. Robblee, W.W. Gu, F.M.F. de Groot, G. Christou, V.L. Pecoraro, S.P. Cramer, V.K. Yachandra, *J. Am. Chem. Soc.* 126, 9946 (2004)
15. Westre, T. E.; Kennepohl, P.; Dewitt, J. G.; Hedman, B.; Hodgson, K. O.; Solomon, E. I. *J. Am. Chem. Soc.* 119, 6297 (1997)
16. S. DeBeer George, P. Brant, and E.I. Solomon, *J. Am. Chem. Soc.* 127, 667 (2005).
17. A Shukla, M. Clanadra, M. Taguchi, A. Kotani, G. Vanko and S.W. Cheong, *Phys. Rev. Lett.* **96**, 077006 (2006).
18. G. Vanko et al. (unpublished).
19. G. Peng, F.M.F. de Groot, K. Hämäläinen, J.A. Moore, X. Wang, M.M. Grush, J.B. Hastings, D.P. Siddons, W.H. Armstrong, O.C. Mullins, S.P. Cramer, *J. Am. Chem. Soc*. 116, 2914 (1994).
20. X. Wang, F. M. F. de Groot, S.P. Cramer, *Phys. Rev. B*. **56**, 4553 (1997).
21. F. M. F. de Groot, S. Pizzini, A. Fontaine, K. Hämäläinen, C. C. Kao, J.B. Hastings, *Phys. Rev. B*. **51**, 1045 (1995)
22. P. Glatzel, L. Jacquamet, U. Bergmann, F. M. F. de Groot and S.P. Cramer, *Inorg. Chem*. **41**, 3121 (2002)
23. U. Bergmann, C. R. Horne, T. J. Collins, J. M. Workman, and S. P. Cramer, *Chem. Phys. Lett.* 302, 119 (1999).
24. J. G. Mesu, et al. *Inorg. Chem*. **45**, 1960 (2006)
25. P. Glatzel, F. M. F. de Groot, O. Manoilova, D. Grandjean, B. M. Weckhuysen, U. Bergmann, and R. Barrea, *Phys. Rev. B.* **72**, 014117 (2005)